PROTEINS: Structure, Function, and Genetics 51:552–561 (2003)

Endogenous Tryptophan Residues of cAPK Regulatory Subunit Type IIβ Reveal Local Variations in Environments and Dynamics

Kerri M. Zawadzki,[1] Chia-Pin Pan,[2] Mary D. Barkley,[2] David Johnson,[3] and Susan S. Taylor[1,4]*
[1]*Department of Chemistry and Biochemistry, University of California, San Diego, La Jolla, California*
[2]*Department of Chemistry, Case Western Reserve University, Cleveland, Ohio*
[3]*Division of Biomedical Sciences, University of California, Riverside, California*
[4]*Howard Hughes Medical Institute, University of California, San Diego, La Jolla, California*

ABSTRACT **The amino terminal dimerization/docking domain and the two-tandem, carboxy-terminal cAMP-binding domains (A and B) of cAMP-dependent protein kinase regulatory (R) subunits are connected by a variable linker region. In addition to providing a docking site for the catalytic subunit, the linker region is a major source of sequence diversity between the R-subunit isoforms. The RIIβ isoform uniquely contains two endogenous tryptophan residues, one at position 58 in the linker region and the other at position 243 in cAMP-binding domain A, which can act as intrinsic reporter groups of their dynamics and microenvironment. Two single-point mutations, W58F and W243F, allowed the local environment of each Trp to be probed using steady-state and time-resolved fluorescence techniques. We report that: (a) the tryptophan fluorescence of the wild-type protein largely reflects Trp243 emission; (2) cAMP selectively quenches Trp243 and thus acts as a cAMP sensor; (3) Trp58 resides in a highly solvated, unstructured, and mobile region of the protein; and (4) Trp243 resides in a stable, folded domain and is relatively buried and rigid within the domain. The use of endogenous Trp residues presents a non-perturbing method for studying R-subunit subdomain characteristics in addition to providing the first biophysical data on the RIIβ linker region. Proteins 2003;51:552–561.**

Key words: cAPK; protein kinase A; regulatory subunit; tryptophan; fluorescence

INTRODUCTION

cAMP-dependent protein kinase A (cAPK) is both the major receptor for cAMP in eukaryotic cells and a critical member of numerous signal transduction pathways. In its inactive state, cAPK exists as a tetramer composed of a regulatory (R) subunit dimer bound to two catalytic (C) subunits. Binding of two cAMP molecules to each R-subunit monomer causes dissociation of the holoenzyme complex and releases an active C-subunit.[1]

R-subunits possess a conserved and well-defined domain structure comprised of an amino-terminal dimerization/docking domain, two-tandem cAMP-binding domains at the carboxy-terminus, and a variable, interconnecting linker region (Fig. 1). The linker region contains a substrate-like inhibitor sequence that docks to the active site cleft of the C-subunit. Two general classes of R-subunits, type I and type II, are known and differ by autophosphorylation, molecular weight, disulfide cross linkage, and cellular localization.[2–4] Each type of R-subunit can be further classified as either α or β, which differ by tissue distribution and antigenicities.[5–7] R-subunit isoforms are not functionally interchangeable. Knockout of the RIα isoform gene in mice is lethal while knockout of the RIIβ isoform gene results in compensatory increases in RIα, a lean phenotype from diminished white adipose tissue, deficits in complex motor behavior, decreased sensitivity to the sedative effects of ethanol consumption, and decreased levels of total C-subunit despite no decrease in levels of cAPK activity.[7–11]

The crystallographic structures of the RIα and RIIβ cAMP-binding domains and the NMR-solution structures of the RIα, RIIα, and RIIβ dimerization/docking domains reveal structural differences between the isoforms[12–14] (Banky et al., forthcoming; Lipsitz, unpublished results). Currently, no high-resolution structural data exists on the linker region of any R-subunit isoform, and the contribution of this subdomain to the observed isoform differences is not known. The linker regions of the various isoforms show the least homology; there are large differences in sequence, length, protein modifications, and potential for protein-protein interactions [Fig. 1(D)].[15–20] It is likely that the diversity of the linker regions underlies, at least, some of the isoform functional differences.

Abbreviations: cAMP, adenosine 3′,5′-cyclic monophosphate; cAPK, cAMP-dependent protein kinase; CD, circular dichroism; C-subunit, catalytic subunit; DAS, decay-associated emission spectra; DTT, dithiothreitol; EDTA, ethylenediaminetetraacetic acid; MOPS, 3-(*N*-morpholino) propanesulfonic acid; SDS, sodium dodecyl sulfate; SDS-PAGE, sodium dodecyl sulfate-polyacrylamide gel electrophoresis; R-subunit, regulatory subunit; WT, wild-type. Buffer A: 25 mM sodium phosphate, 150 mM NaCl, 0.1 mM EDTA, 0.1 mM DTT, pH 7.4.

Grant sponsor: NIH; Grant numbers: GM34921, GM08326-10.

*Correspondence to: Susan S. Taylor, 9500 Gilman Dr., 0654, La Jolla, CA 92093-0654. E-mail: staylor@ucsd.edu

Received 19 July 2002; Accepted 28 October 2002

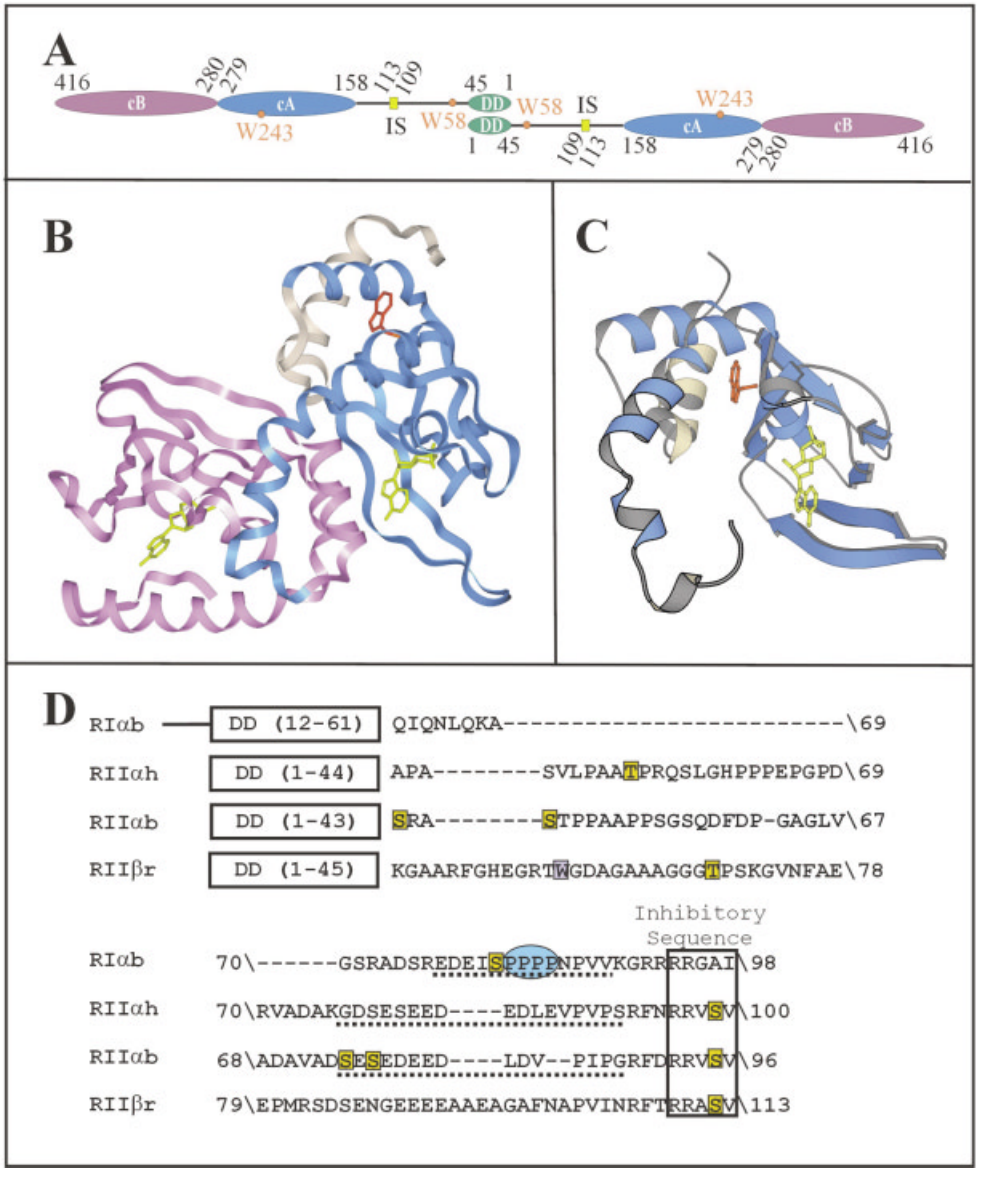

Fig. 1. Schematic diagram and summary of the domain structure and mutants of the type IIβ regulatory subunit of the cAMP-dependent protein kinase (PDB accession code 1CX4). **A:** Cartoon demonstrating location of the N-terminal dimerization/docking domain (green), autoinhibitory region (yellow), cAMP-binding domains A and B (blue and purple, respectively), and intrinsic tryptophans (orange circles). **B:** Ribbon diagram showing the location of Trp243 in the Δ1-111 crystallographic structure of RIIβ. **C:** Close-up diagram highlighting the local environment of Trp243. **D:** Sequence comparison of R-subunit linker regions demonstrates low homology between the isoforms. The species listed are bovine (b), human (h), and rat (r). The sites of phosphorylation are highlighted in yellow, the endogenous Trp residue is in purple, the putative PEST sequences are highlighted with dashed lines, and the putative Grb2 binding site is shown in blue.

Time-resolved fluorescence anisotropy experiments on the RIα linker region and other subdomains have previously been carried out using fluorescent probes attached to cysteines engineered into the protein. These studies suggest that the RIα linker region is highly flexible.[21] One drawback of the previous RIα anisotropy experiments is that the protein was modified by addition of an extrinsic fluorescent probe, which may perturb the structure and/or dynamics of the protein. The development of a nonperturbing method is necessary for an unambiguous understanding of the dynamics of the linker region.

Of the four known R-subunits, only the linker region of the RIIβ isoform contains an endogenous tryptophan residue (Trp58) [Fig. 1(D)] that could act as an intrinsic reporter group. Consequently, we studied the anisotropy decay of RIIβ to determine the conformational flexibility of a portion of the linker region. Because there is also a second endogenous tryptophan at position 243 in cAMP-binding domain A (Fig. 1), we prepared and studied in parallel two Trp-to-Phe mutant proteins (W58F and W243F) to characterize the emission properties of each Trp residue. The results described here present a clearly

non-perturbing method of studying the R-subunit linker regions. Furthermore, these studies represent the first biophysical analysis of the linker region of RIIβ, the predominant R-subunit isoform in brain and adipose tissue. We report that Trp58 resides in a highly solvated, unstructured, and mobile region of the protein while Trp243 resides in a stable, folded domain, is relatively buried and rigid within the domain, and behaves as a cAMP sensor.

MATERIALS AND METHODS

Mutagenesis

The gene coding for the full-length rat type IIβ R subunit was obtained as a pRSET B (Invitrogen, Carlsbad, CA) expression cassette.[22] Single-stranded DNA of this gene was prepared and used in oligonucleotide-directed mutagenesis via the Kunkel method. Oligonucleotides were purchased from GenBase Inc. (San Diego, CA). Transformation of the DNA into competent DH5α cells (Gibco BRL, Carlsbad, CA), isolation of the plasmid, and verification of the DNA sequence were performed as previously described.[22]

Expression and Purification

Proteins were expressed in *Escherichia coli* BL21 (DE3) cells (Novagen, Madison, WI) and purified using cAMP-agarose resin.[22] Cyclic nucleotide-free protein was obtained by eluting RIIβ from the resin with 10 mM cGMP instead of cAMP (J. Jones, personal communication). Typical yields of the proteins were 2–4 mg/L of cell culture.

Protein Characterizations

The cAMP:R monomer stoichiometry was determined by UV spectrometry.[23] Protein aliquots (8 μM) were prepared with protein free of unbound cAMP. Circular dichroism (CD) measurements were acquired using an AVIV (Lakewood, NJ) 202 CD spectropolarimeter. Fluorescence measurements were carried out with a SPEX (Edison, NJ) Fluoromax-2 spectrofluorometer.

Acrylamide Quenching of Tryptophan Fluorescence

The tryptophan fluorescence of the samples (1 μM in buffer A) was quenched with acrylamide (0–0.30 M). The emission intensity with excitation at 295 nm was monitored near the maximum emission wavelength of each protein (WT, 334 nm; W58F, 330 nm; W243F, 353 nm). The fluorescence quenching data were plotted using the Stern-Volmer equation: $F_o/F = 1 + K_{SV}$ [Q], where F_o and F are the emission intensity in the absence and presence of quencher Q, respectively, and K_{SV} is the Stern-Volmer quenching constant.[24]

Urea Unfolding of the RIIβ Subunits

A stock solution of 8.5 M urea was prepared in buffer A. Amberlite MB-150 (Sigma, St. Louis, MO) mixed-bed exchanger was added to this solution and stirred for 1 h to remove ionic urea degradation products. The urea solution was filtered and frozen at −20°C.

Proteins (1 μM) were unfolded in various concentrations of urea for 2 h at room temperature and monitored by both steady-state fluorescence and CD. Overnight incubation produced no additional changes in the fluorescence emission or CD spectra. Fractional unfolding curves were constructed assuming a two-state model and using $F_U = 1 - [(R - R_U)/(R_F - R_U)]$, where F_U is the fraction of the unfolded protein, F_N is the fraction of folded protein, R is the fluorescence or CD measurement, and R_F and R_U represent the values of R for the folded and unfolded states, respectively.[25] For unfolding monitored by CD, R is the mean residue ellipticity at 222 nm. For unfolding monitored by fluorescence, R is the observed ratio of intensity at 356/334 nm with excitation at 295 nm.

Free energy of denaturation, ΔG_U, values at each urea concentration in the transition region of the denaturation curves were calculated from the fraction of folded and unfolded protein according to $-RT \ln (F_N/F_U) = \Delta G_U$. The ΔG_U for the unfolded protein at zero concentration of denaturant, ΔG_U^{H2O}, was calculated according to the linear extrapolation method.[25]

Quantum Yield Determinations

Fluorescence quantum yields, Φ, were measured relative to tryptophan (Sigma, recrystallized four times from 70% ethanol) using a value of 0.14 in water at 25°C.[26] Emission spectra (4-nm band pass) were measured using a SLM 8000C (SLM Instruments, Urbana, IL) at 300 nm excitation wavelength (4-nm band pass) to avoid cAMP absorbance. Sample absorbance at 300 nm was <0.05 in buffer A using 3-mm path length cuvettes. The excitation and emission polarizers were set at 54.7° and 0°, respectively, to eliminate anisotropic effects. Spectra were corrected using correction factors determined with a standard lamp (Optronics, Orlando, FL).

Time-Resolved Fluorescence

Fluorescence lifetimes were measured by time-correlated single photon counting at 25°C. The excitation source was a Spectra-Physics (Mountain View, CA) Tsunami mode-locked Ti-sapphire laser pumped with a Millennia diode-pumped Nd-YVO_4 laser. The 80-MHz output of the Tsunami was passed through a Spectra-Physics Model 3980/3985 pulse selector set at 4 MHz. Wavelength and laser stability were monitored by an IST-Rees (Horseheads, NY) LSA E201 laser spectrum analyzer. The wavelength was set at 900 nm and the pulse width was 2 ps. The laser beam was passed through a GWU HG flexible harmonic generator (Spectra-Physics). The tripled output at 300 nm was focussed by two cylindrical lenses and used to excite the sample. The doubled output at 450 nm was passed through a Pellin Broca prism (CVI Laser Corp., Albuquerque, NM) to remove the fundamental and detected by an ET2010 silicon pin detector (Electro-Optics Technology, Traverse City, MI). The inverted detector output was delayed and used as the stop timing signal. The fluorescence emission was detected by a cooled Hamamatsu (Hamamatsu, Japan) R3809U-50 microchannel plate photomultiplier. The photomultiplier output was amplified by

a Model 6954 fast pulse preamplifier (Philips Scientific, Ramsey, NJ) and used as the start timing signal. A SPC-330-12 PC module (Becker & Hickl GmbH Intelligent Measurement and Control Systems, Berlin, Germany) installed in a 266-MHz Micron computer was used for the photon counting electronics.

The exciting light was vertically polarized. The emission polarizer (HNP'B, Polaroid, Cambridge, MA) was set at 55° for lifetime experiments. Emission wavelength (8-nm band pass) was selected by an Instruments SA (Edison, NJ) H-10 monochromator. A DPU-2.5 optical depolarizer (Optics for Research, Caldwell, NJ) was placed before the emission monochromator to eliminate polarization dependence of the detection train, so that G $\approx$ 1 for anisotropy experiments. Fluorescence decays were acquired contemporaneously with a lamp profile in 1,024 channels of 9.8 and 24.4 ps/channel. A scattering solution of dilute coffee creamer was used for the lamp profile. Decay curves were deconvolved using the Beechem global program.[27] Goodness of fit was judged by reduced chi-square, χ^2_r, and the autocorrelation function of the weighted residuals.

Fluorescence intensity decays $I(t)$ were fit to a sum of exponentials

$$I(t) = \sum_i \alpha_i \exp(-t/\tau_i) \quad (1)$$

with relative amplitudes α_i and lifetimes τ_i. Decay curves acquired at different emission wavelengths were deconvolved simultaneously, assuming that lifetimes but not amplitudes were independent of wavelength. A 4–16-ps component representing scattered light was included in the analysis. Scattered light contributed $\leq$1.4% of the total intensity for wild type and W58F mutant at 310–390 nm emission wavelength and $\leq$5.5% for W243F mutant at 340–390 nm emission wavelength. Amplitude-weighted lifetime $\bar{\tau} = \Sigma_i \alpha_i \tau_i$. Intensity-weighted lifetime $\langle\tau\rangle = \Sigma_i f_i \tau_i$, where $f_i = \alpha_i \tau_i / \Sigma_i \alpha_i \tau_i$ is the fractional intensity. Decay-associated emission spectra $F_i(\lambda)$ were calculated by combining the steady-state emission spectrum $F(\lambda)$ and time-resolved data.

$$F_i(\lambda) = \alpha_i(\lambda) \tau_i F(\lambda) / \Sigma_i \alpha_i(\lambda) \tau_i \quad (2)$$

In constructing the DAS, the steady-state emission spectrum of wild type was normalized to one at the peak and the steady-state spectra of W58F and W273F mutants were scaled relative to wild type at equal protein concentrations based on absorbance at 300 nm. Assuming that Trp273 and Trp58 have equal extinction coefficients, wild type has twice the extinction coefficient of the single tryptophan mutants.

Fluorescence anisotropy decays $r(t)$ were fit to a sum of exponentials

$$r(t) = \sum_i \beta_i \exp(-t/\phi_i) \quad (3)$$

with pre-exponentials β_i and rotational correlation times ϕ_i. The initial anisotropy $r(0) = \Sigma_i \beta_i$. Individual polarized decays $I_{VV}(t)$ and $I_{VH}(t)$ were deconvolved simultaneously with a magic angle decay $I(t)$

$$I_{VV}(t) = I(t)[1 + 2\, r(t)]/3 \quad (4a)$$

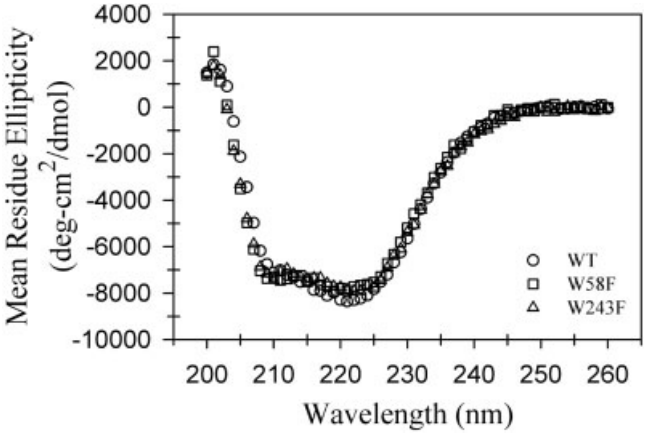

Fig. 2. Far-UV circular dichroism spectra of wild-type RIIβ (circles), W58F (squares), and W243F (triangles). Samples (1 μM) were scanned from 260 to 200 nm at 25°C in buffer A. The mean residue ellipticity is shown as a function of wavelength.

$$I_{VH}(t) = G\, I(t)[1 - r(t)]/3 \quad (4b)$$

where the correction factor G $\approx$ 1 in our instrument. Anisotropy data sets acquired on 10- and 25-ns time scales were included in the global analysis. The global analysis constrained the lifetimes to be the same in all the decay curves, and the pre-exponentials and rotational correlation times to be the same in the polarized decays.

RESULTS

Characterization of Wild-Type RIIβ and the Tryptophan Mutants.

Because the replacement of tryptophan residues with phenylalanine affects protein absorbance, molar extinction coefficients at 280 nm, ϵ_{280}, were determined by amino acid analysis for all three proteins in their native, cAMP-bound states. The ϵ_{280} values of 3.40, 3.09, and 3.29 $\times$ 10^4 M^{-1} cm^{-1} for wild-type, W58F, and W243F RIIβ were used in protein concentration determinations unless otherwise noted. The tryptophan mutations did not affect cAMP binding, as the mol cAMP:mol R monomer stoichiometry ranged between 1.8–2.2 for all three proteins, and the mutants were fully capable of inhibiting the protein kinase A C-subunit (data not shown). The wild-type, W58F, and W243F RIIβ proteins also had identical CD spectra, indicating that the mutations did not significantly affect the proteins' secondary structure (Fig. 2).

Urea Denaturation Monitored by Circular Dichroism

Plots of fraction of protein unfolded (F_U) at various urea concentrations showed essentially the same concentrations of the transition midpoints, C_m, and slopes of the transition region, m, for wild-type, W58F, and W243F RIIβ, signifying that the mutations did not have a major effect on the relative global stability of the proteins or the cooperativity of the unfolding process, respectively (Table I).

TABLE I. Unfolding Parameters of Wild-Type and Mutant RIIβ Subunits[†]

Protein	ΔG_U^{H2O} (kcal/mol)	C_m (M)[a]	m (kcal/mol · M)
Circular Dichroism			
WT	3.5 ± 0.3	4.62 ± 0.06	0.77 ± 0.06
W58F	3.8 ± 0.8	4.3 ± 0.2	0.9 ± 0.1
W243F	4.0 ± 0.7	4.3 ± 0.2	0.9 ± 0.2
Fluorescence			
WT	10.4 ± 0.6	5.40 ± 0.03	1.9 ± 0.1
W58F	8.9 ± 0.4	5.0 ± 0.1	1.8 ± 0.1
W243F	n.d.	n.d.	n.d.

[†]Parameters calculated using $\Delta G_U = \Delta G_U^{H2O} - m[\text{urea}]$.
[a]$C_m = \Delta G_U^{H2O} / m$.

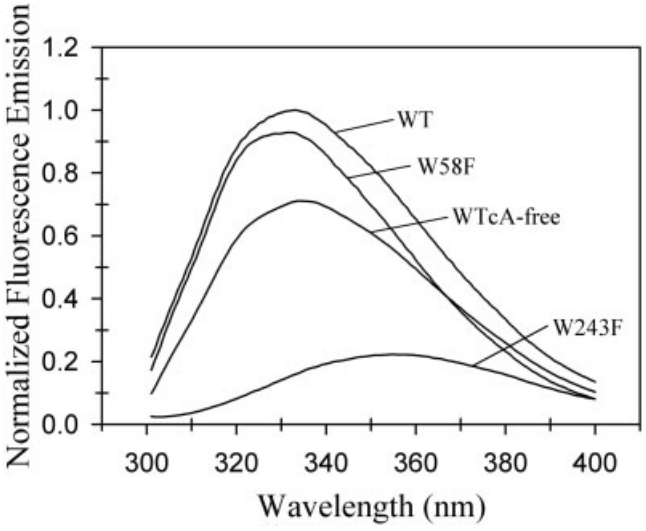

Fig. 3. Comparison of the technical fluorescence emission spectra of wild-type, a cAMP-free wild-type (WTcA-free), and tryptophan mutants of RIIβ. Samples (1 μM) were excited at 295 nm at 25°C in buffer A.

Fluorescence Spectra

Comparison of the intensity of fluorescence emission from each of the proteins revealed that Trp243 contributes most of the total wild-type fluorescence (Fig. 3). The quantum yield of Trp243 in the W58F mutant is 10 times the value of Trp58 in the W243F mutant (Table II). The quantum yield of wild-type RIIβ is only half that of the W58F mutant, as expected if both tryptophans have the same molar absorptivity, but Trp58 emits very weakly compared to Trp243. Trp243 is clearly the major fluorescence emitter in RIIβ. Additionally, cAMP-free wild-type RIIβ (WTcA-free) is a weaker fluorescence emitter than the cAMP-bound wild-type protein. This suggests that the endogenous Trp residues, primarily Trp243, are sensitive to the presence of cAMP and are thus cAMP-sensors.

Differences in the local environment of each tryptophan residue were revealed in the maximum emission wavelength, λ_{max}, of each protein (Table II). The λ_{max} value of W243F was red shifted >13 nm relative to the λ_{max} values of wild-type RIIβ and W58F mutant protein and indicates that Trp58 exists in a more polar environment than Trp243.

Fluorescence Lifetime

The lifetimes τ_i of the three proteins are about the same and independent of emission wavelength (Table III). In both single tryptophan mutants, the relative amplitudes α_i are also independent of emission wavelength, indicating that the emission spectra of the three lifetime components DAS_i have the same spectral shape. In wild-type RIIβ, the amplitudes vary with emission wavelength, consistent with two tryptophans having different emission spectra. Figure 4 shows the DAS of the long and medium lifetime components of the mutants relative to wild-type type RIIβ (Fig. 4, circles). The short lifetime component contributes only a small fraction of the steady-state intensity and is not shown. For the W58F mutant protein (Fig. 4, squares), the 5.6-ns DAS has about eightfold greater intensity than the 2.7-ns DAS, with both emission maxima at about 330 nm. For the W243F mutant protein (Fig. 4, triangles), the 5.7- and 2.1-ns DAS have equal intensity and emission maxima at about 350 nm. For wild-type RIIβ (Fig. 4, circles), the DAS_i contain contributions from the lifetime components i of both tryptophans, according to their relative intensity. The 5.5-ns DAS of wild-type protein comprises mostly the 5.6-ns DAS of the W58F mutant protein plus a small contribution from the 5.7-ns DAS of the W243F mutant protein, which shifts the emission maximum slightly to the red to about 335 nm. In contrast, the 2.1-ns DAS of wild-type protein comprises more equal contributions from the 2.7-ns DAS of the W58F mutant protein and the 2.1-ns DAS of the W243F mutant protein, which broadens the emission spectrum and shifts it to about 345 nm. The DAS for the three proteins confirm that the two tryptophans in wild-type RIIβ emit independently.

The radiative rate, k_r, for Trp243 is comparable to k_r values for 3-methylindole, tryptophan zwitterion, and *N*-acetyltryptophanamide ($4-6 \times 10^7$ s^{-1}),[28] but k_r for Trp58 is an order of magnitude less (Table II). The apparent low k_r value of the W243F mutant indicates that the low quantum yield of Trp58 is presumably due to static quenching of tryptophan fluorescence by ground-state interactions.[29]

Acrylamide Quenching

The Stern-Volmer plots for acrylamide quenching of the two single tryptophan mutants' fluorescence emission were linear, consistent with a dynamic quenching process. The bimolecular quenching rate constant, which represents solute accessibility, was more than six-fold greater for the W243F mutant than for the W58F mutant (Table II), indicating that Trp58 is significantly more solute accessible than Trp243.

These differences in solvent accessibility were then compared to theoretical quenching efficiencies derived from known R-subunit structure models. The theoretical diffusion-controlled rate constant $k_d = 4.5 \times 10^9$ M^{-1} s^{-1} was estimated for acrylamide and RIIβ from the Smoluchowski equation. The translational diffusion coefficient of RIIβ was estimated by the computer program HYDRO,[30] using bead models of the RIIα structure.[31] The low quenching efficiency, f_q, for Trp243, is consistent with a buried

TABLE II. Steady-State Fluorescence Data†

Protein	λ_{max}(nm)[a]	Φ	k_r ($\times 10^7$ s^{-1})[b]	K_{SV} (M^{-1})	k_q ($\times 10^9$ M^{-1} s^{-1})[c]	f_q[d]
WT	335	0.074 ± 0.001		1.3 ± 0.2		
W58F	332	0.15 ± 0.02	3.3 ± 0.5	1.01 ± 0.08	0.19 ± 0.03	0.042
W243F	348	0.015 ± 0.002	0.8 ± 0.1	4.2 ± 0.3	1.2 ± 0.1	0.27

†Errors are standard deviations of 3–5 experiments.
[a]Corrected emission spectra.
[b]Calculated from $k_r = \Phi / \bar{\tau}$ with data from Table IV.
[c]Calculated from $k_q = K_{SV} / \langle\tau\rangle$ with data from Table IV.
[d]Calculated from $f_q = k_q/k_d$ with $k_d = 4.5 \times 10^9$ M^{-1} s^{-1} estimated as described in the text.

TABLE III. Lifetime Data†

Protein	α_1	τ_1 (ns)	α_2	τ_2 (ns)	τ_3 (ns)	$\bar{\tau}$ (ns)	$\langle\tau\rangle$ (ns)	χr^2
WT[a]	0.66–0.44	5.52	0.22–0.30	2.08	0.36			1.08
W58F[a]	0.69 ± 0.06	5.59	0.20 ± 0.04	2.71	0.50	4.5 ± 0.3	5.2 ± 0.6	1.06
W243F								
Buffer[b]	0.14 ± 0.01	5.70	0.40 ± 0.03	2.15	0.39	1.9 ± 0.1	3.5 ± 0.3	1.14
35% glycerol[c]	0.242 ± 0.008	5.40	0.41 ± 0.01	2.15	0.41	2.19 ± 0.05	4.1 ± 0.1	1.60

†$\Sigma_i \alpha_i = 1$. Decays were fit to three exponentials plus a term for scattered light.
[a]Global analysis of data from 310–390 nm emission wavelength, 10-nm intervals.
[b]Global analysis of data from 340–390 nm emission wavelength, 10-nm intervals.
[c]Emission wavelength 350 nm.

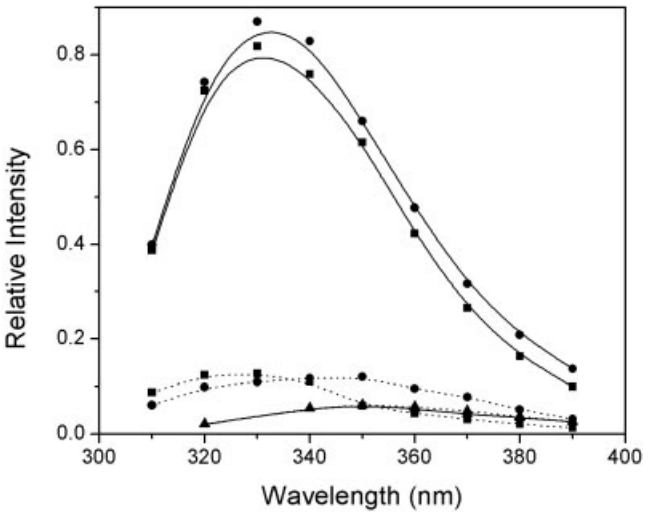

Fig. 4. Decay-associated emission spectra of wild-type and tryptophan mutants of RIIβ. Long (—) and medium (…) lifetime components; wild-type (circles), W58F (squares), and W243F (triangles).

tryptophan in the W58F mutant while the much higher f_q for Trp58 indicates an exposed tryptophan in the W243F mutant (Table II).

Emission Anisotropy

Time-resolved emission anisotropy of the three proteins was measured to examine the mobility of the two tryptophans (Table IV). The anisotropy decay of wild-type RIIβ required a two exponential fit and is dominated by a 39-ns correlation time that likely reflects whole-body motion of the protein. Modeling RIIβ as described above and using HYDRO to calculate the five rotational correlation times of an anisotropic rigid body tested the validity of this supposition. A set of correlation times was calculated using the sets of dimensions for each of the two RII cAMP-binding domain structures (RIIα by neutron scattering[31] and RIIβ by crystallography[13]). For both cases, the dimensions for the dimerization/docking domain and linker region were taken from the neutron scattering structure of RIIα. Three unique ϕ_i values, 45, 23, and 9.3 ns, were obtained using the ellipsoidal dimensions (44–45, 29, and 15–16 Å) determined by neutron scattering. Using the slightly larger ellipsoidal dimensions (50, 36, and 30 Å) from the crystal structure yielded 61, 41, and 21-ns ϕ_i values. The two longer calculated correlation times in each set of ϕ_i values are most likely due to end-over-end tumbling of the dumbbell-like structures. The experimental value of 39-ns is within the range of calculated values, considering the uncertainty in determining correlation times 6–12 times longer than the intensity-weighted lifetime, and thus ϕ_1 represents protein whole-body motion. Additionally, a global analysis of the anisotropy data for the three proteins on two time scales constraining one correlation time to be the same in all the data sets gave ϕ_1 = 40.7 ns with global χ_r^2 = 1.40, indicating that the long rotational correlation time is the same in the three proteins. The short calculated correlation time is most likely governed by faster rotations about the long axis of RIIβ.

The anisotropy data for the W58F mutant protein gave an acceptable fit to a single exponential, but assuming two rotational correlation times resulted in a slightly lower χ_r^2 and more random autocorrelation functions (Table IV). Based on relative values of the pre-exponentials β_i, the ϕ_1 value accounts for 96% of Trp243 mobility. The initial anisotropy $r(0)$ = 0.27 approaches the limiting value of 0.29 (at 300 nm excitation wavelength) for tryptophan

TABLE IV. Anisotropy Data[†]

Protein	β_1	ϕ_1 (ns)	β_2	ϕ_2 (ns)	$r(0)$	χ_r^2
WT[a]	0.22	38.8	0.04	0.30	0.26	1.30
W58F[b]	0.26	38.0	0.01	1.70	0.27	1.37
W243F						
Buffer[c]	0.09	30.0	0.14	0.80	0.23	1.52
35% glycerol[d]	0.11	76.3	0.14	1.60	0.25	1.60

[†]Global analysis of data from 10- and 24-ns time scales, 350-nm emission wavelength. Lifetimes recovered from anisotropy data: [a]$\tau_1 = 5.50$ ns, $\tau_2 = 2.13$ ns, $\tau_3 = 0.36$ ns. [b]$\tau_1 = 5.57$ ns, $\tau_2 = 2.54$ ns, $\tau_3 = 0.39$ ns. [c]$\tau_1 = 5.70$ ns, $\tau_2 = 2.05$ ns, $\tau_3 = 0.35$ ns. [d]Data in Table III.

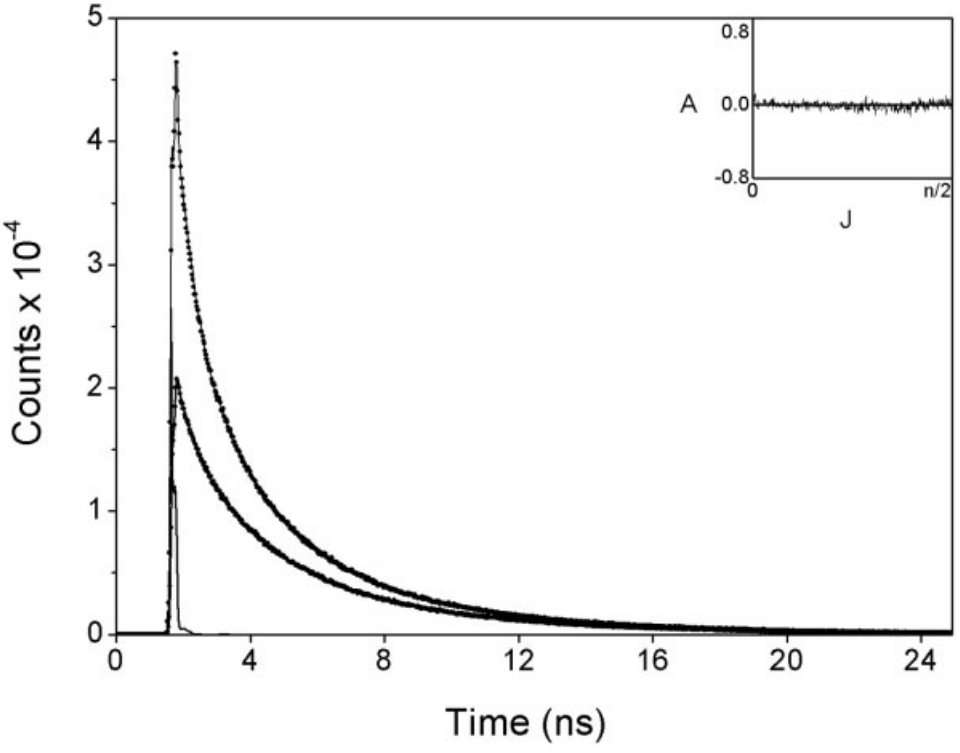

Fig. 5. Fluorescence anisotropy decay data for W243F mutant in 35% glycerol. Solid curve is the instrument response, points are $I_{VV}(t)$ (higher) and $I_{VH}(t)$ (lower), and smooth curves through points are best fits from global analysis of 25-ns data set. The autocorrelation function of the weighted residuals (**inset**) is shown for $I_{VV}(t)$. Decay parameters:$\tau_1 = 5.57$ ns ($\alpha_1 = 0.22$), $\tau_2 = 2.34$ ns ($\alpha_2 = 0.43$), $\tau_3 = 0.49$ ns ($\alpha_3 = 0.35$); $\phi_1 = 48.0$ ns ($\beta_1 = 0.13$), $\phi_2 = 1.40$ ns ($\beta_2 = 0.14$); global $\chi_r^2 = 1.12$.

zwitterion in water,[32] indicating that there is little or no detectable internal motion.

The anisotropy decays for the W243F mutant clearly required two exponentials to fit the data with rotational correlation times of 30 and 0.8 ns. Based on relative β_i values, the fraction of Trp58 anisotropy decay due to whole-body rotational diffusion is about 40% (Table IV). The 0.8-ns correlation time is due to internal mobility of Trp58. Because rotational correlation times are proportional to viscosity, viscosity dependence is expected if $\phi_2 =$ 0.8 ns represents protein flexibility in the vicinity of an exposed tryptophan and not depolarization due to energy transfer between the two Trp58 residues in the RIIβ dimer. Anisotropy decay experiments were conducted in 35% glycerol (Fig. 5). The 2.5- and 2-fold increases for ϕ_1 and ϕ_2, respectively, demonstrated a viscosity dependence for both correlation times. Mobility of the indole side chain of Trp58 is also evidenced by an $r(0)$ value of 0.23, indicating as much as 20% unresolved fast motion.

Urea Denaturation Monitored by Fluorescence

The urea-induced unfolding of the three RIIβ proteins was followed by intrinsic fluorescence to monitor unfolding in the local environments of the tryptophan residues. The fluorescence spectra for wild-type RIIβ and the W58F mutant both showed a decrease in intensity and a large red-shift in λ_{max} as urea concentrations increase while the spectra of the W243F mutant showed an increase in intensity but no major shift in λ_{max} (data not shown). The F_U plots (Fig. 6) for wild-type RIIβ and the W58F mutant were both sigmoidal, indicating the ability of these proteins to monitor conformational changes within RIIβ, and gave comparable values for C_m and slope of the transition

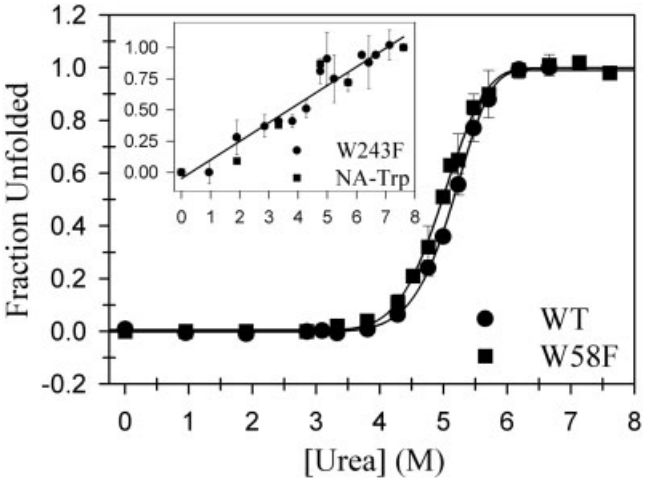

Fig. 6. Urea-induced fraction unfolded curves for the RIIβ-subunits as monitored by fluorescence. Wild-type (circles) and W58F (squares) are shown in the foreground. **Inset:** The relative intensity plots for W243F (circles) and N-acetyltryptophan (NA-Trp, squares).

region (Table I). The W243F mutant profile, however, yielded a linear F_U plot (Fig. 6, inset).

The linear increase in fluorescence intensity from free tryptophan or tryptophan derivatives, such as N-acetyltryptophan, upon addition of urea is well documented[33] and probably due to the decreased water activity and slower water quenching rate when urea is added to the buffer.[28] A linear intensity vs. urea concentration plot would be expected if the fluorophore is solvent accessible, such as when tryptophan is in an unstructured region of the protein. This plot is linear for N-acetyltryptophan and comparable to the plot for the W243F mutant (Fig. 6, inset), suggesting that Trp58 sits in an unstructured region of RIIβ.

DISCUSSION

The linker region is the most variable region between the isoforms and is, therefore, likely to contribute significantly to the unique physiological properties of the R-subunits [Fig. 1(D)]. To understand why the R-subunit isoforms exhibit unique and non-redundant physiological functions, we must endeavor to understand the structure and dynamics of each subdomain, including the linker regions. Steady-state and time-resolved fluorescence experiments using wild-type and mutated RIIβ proteins containing a single tryptophan showed that the two endogenous tryptophans (Trp58 in the linker region and Trp243 in cAMP-binding domain A) have very different environments and dynamics. These studies provided us with insight into the properties of the subdomains in which the tryptophans reside and the first biophysical characterization of the RIIβ isoform. The R-subunit endogenous tryptophan residues proved to be a valuable alternative to extrinsic fluorescent probes in R-subunit fluorescence anisotropy experiments.

Trp243 is buried in a stable, structured domain. The high homology in both sequence and structure between the cAMP-binding domains of RIIβ and RIα allows us to make comparisons between these two isoforms. Sequence alignment shows that Trp243 in RIIβ and Trp222 in RIα are homologous while the crystallographic structures of the cAMP-binding domains showed Trp243 and Trp222 to be situated in β-strand 8 of the compact β-barrels of the A binding domain [Fig. 1(C)].[12,13] Like its RIIβ counterpart, Trp222 in RIα was also found to be the largest contributor to fluorescence emission from the wild-type protein, situated in a hydrophobic environment, and most shielded from solvent.[34] Furthermore, the previous time-resolved anisotropy experiments on RIα using extrinsic fluorescent probes attached at various engineered sites throughout the protein showed that probes directed to cAMP-binding domain A were relatively rigid compared to probes directed to the linker region.[21] The characteristic of a rigid and well-folded cAMP-binding domain appears to be conserved within the R-subunit family.

An interesting difference between the RIIα and RIIβ isoforms is the sensitivity of the endogenous tryptophan residues to the presence of cAMP. Upon removal of cAMP, the fluorescence emission of the RIIβ tryptophan residues was quenched while the emission from the RIIα tryptophan residue (Trp226 in cAMP-binding domain A) was unaffected.[35] Considering that the single RIIα tryptophan is homologous to Trp243 of RIIβ, the primary fluorescence emitter in RIIβ, this was an unexpected difference between the isoforms.

In contrast to Trp243, Trp58 is in a highly solvated, unstructured, and mobile region of RIIβ. Our results agree well with the high protease sensitivity of this region.[36,37] The flexible nature of the linker region also correlates well with the time-resolved fluorescence anisotropy data for RIα.[21] Additionally, the small-angle scattering data from RIIα suggested that this region is extended, which may correlate with both solvent accessibility and little structure.[31] The characteristics of high solvent accessibility and little structure in the linker region, in contrast to the two stable domains at the N- and C-terminus, appear to be conserved within the R-subunit family and define a protein with a high degree of plasticity.

The linker region is a major source of diversity between the R-subunit isoforms and introduces considerable flexibility within the protein. The degree of flexibility may differ with each isoform, thus helping to produce the observed in vivo physiological and functional isoform differences.[31] Glycine residues, which are necessary for significant flexibility, are more abundant in type II R-subunits and may lead to a linker region that is more flexible than that of the type I isoforms. Flexibility in the linker region may be a critical determinant of cAPK function by (1) providing a degree of mobility in the type II isoforms despite their subcellular localization via the A-Kinase-Anchoring-Domains (AKAPs),[38] (2) enhancing and/or facilitating the phosphorylation of adjacent membrane-associated targets,[21] and (3) directing the R-subunit NH_2-terminal domain to assume its proper, isoform specific orientation when in the cAPK holoenzyme complex.[39–41]

This study highlights the distinct characteristics and properties of the two endogenous RIIβ tryptophans and their respective subdomains, provides the first biophysical analysis of the RIIβ linker region, and establishes the use of R-subunit endogenous tryptophan residues as probes of protein conformation and dynamics. The fact that each of the residues is located in separate domains provides us with an excellent tool for further studies of RIIβ to monitor conformational changes within either domain upon phosphorylation or binding of the C-subunit, AKAPs, or cAMP.

ACKNOWLEDGMENTS

We thank Brad Nolen for assistance in the preparation of Figure 1. We also thank Dr. Lora Burns, Dr. John Finke, and Dr. Patricia Jennings for technical advice, helpful discussions, and critical review of the manuscript. This work was supported by an NIH grant to S.S.T. (GM34921). K.M.Z. was supported by a Department of Education Graduate Assistance in Areas of National Need (GAANN) Fellowship and by NIH Training Grant GM08326-10.

REFERENCES

1. Ogreid D, Døskeland SO. The kinetics of the interaction between cyclic AMP and the regulatory moiety of protein kinase II. Evidence for interaction between the binding sites for cyclic AMP. FEBS Lett 1981;129:282–286.
2. Corbin JD, Keely SL, Park CR. The distribution and dissociation of cyclic adenosine 3′:5′-monophosphate-dependent protein kinases in adipose, cardiac, and other tissues. J Biol Chem 1975;250: 218–225.
3. De Camilli P, Moretti M, Donini SD, Walter U, Lohmann SM. Heterogeneous distribution of the cAMP receptor protein RII in the nervous system: evidence for its intracellular accumulation on microtubules, microtubule-organizing centers, and in the area of the golgi complex. J Cell Biol 1986;103:189–203.
4. Rubin CS, Rangel-Aldao R, Sarkar D, Erlichman J, Fleischer N. Characterization and comparison of membrane-associated and cytosolic cAMP-dependent protein kinases. Physicochemical and immunological studies on bovine cerebral cortex protein kinases. J Biol Chem 1979;254:3797–3805.
5. Hofmann F, Beavo JA, Bechtel PJ, Krebs EG. Comparison of adenosine 3′:5′-monophosphate-dependent protein kinases from rabbit skeletal and bovine heart muscle. J Biol Chem 1975;250: 7795–7801.
6. Scott JD, Glaccum MB, Zoller MJ, Uhler MD, Helfman DM, McKnight GS, Krebs EG. The molecular cloning of a type II regulatory subunit of the cAMP-dependent protein kinase from rat skeletal muscle and mouse brain. Proc Natl Acad Sci USA 1987;84:5192–5196.
7. Cummings DE, Brandon EP, Planas JV, Motamed K, Idzerda RL, McKnight GS. Genetically lean mice result from targeted disruption of the RII beta subunit of protein kinase A. Nature 1996;382: 622–626.
8. Amieux PS, Cummings DE, Motamed K, Brandon EP, Wailes LA, Le K, Idzerda RL, McKnight GS. Compensatory regulation of RIalpha protein levels in protein kinase A mutant mice. J Biol Chem 1997;272:3993–3998.
9. Brandon EP, Idzerda RL, McKnight GS. PKA isoforms, neural pathways, and behaviour: Making the connection. Curr Opin Neurobiol 1997;7:397–403.
10. Thiele TE, Willis B, Stadler J, Reynolds JG, Bernstein IL, McKnight GS. High ethanol consupmtion and low sensitivity to ethanol-induced sedation in protein kinase A-mutant mice. J Neurosci 2000;20:RC75.
11. Planas JV, Cummings DE, Idzerda RL, McKnight GS. Mutation of the RIIbeta subunit of protein kinase a differentially affects lipolysis but not gene induction in white adipose tissue. J Biol Chem 1999;274:36281–36287.
12. Su Y, Dostmann WR, Herberg FW, Durick K, Xuong NH, Ten Eyck L, Taylor SS, Varughese KI. Regulatory subunit of protein kinase A: structure of deletion mutant with cAMP binding domains. Science 1995;269:807–813.
13. Diller TC, Madhusudan, Xuong, N-h, Taylor, S.S. Molecular basis for regulatory subunit diversity in cAMP-dependent protein kinase: crystal structure of the type IIb regulatory subunit. Structure 2001;9:73–82.
14. Newlon MR, M, Morikis, D, Carr, DW, Westphal, R, Scott, JD, Jennings, PA. A novel mechanism of PKA anchoring revealed by solution structures of anchoring complexes. EMBO J 2001;20:1651–1662.
15. Tortora G, Damiano V, Bianco C, Baldassarre G, Bianco AR, Lanfrancone L, Pelicci PG, Ciardiello F. The RIalpha subunit of protein kinase A (PKA) binds to Grb2 and allows PKA interaction with the activated EGF-receptor. Oncogene 1997;14:923–928.
16. Rosen OM, Erlichman J. Reversible autophosphorylation of a cyclic 3′:5′-AMP-dependent protein kinase from bovine cardiac muscle. J Biol Chem 1975;250:7788–7794.
17. Carmichael DF, Geahlen RL, Allen SM, Krebs EG. Type II regulatory subunit of cAMP-dependent protein kinase. Phosphorylation by casein kinase II at a site that is also phosphorylated in vivo. J Biol Chem 1982;257:10440–10445.
18. Hemmings BA, Aitken A, Cohen P, Rymond M, Hofmann F. Phosphorylation of the type-II regulatory subunit of cyclic-AMP-dependent protein kinase by glycogen synthase kinase 3 and glycogen synthase kinase 5. Eur J Biochem 1982;127:473–481.
19. Keryer G, Luo Z, Cavadore JC, Erlichman J, Bornens M. Phosphorylation of the regulatory subunit of type II beta camp-dependent protein kinase by cyclin b/p34cdc2 kinase impairs its binding to microtubule-associated protein 2. Proc Natl Acad Sci U S A 1993;90:5418–5422.
20. Keryer G, Yassenko M, Labbe JC, Castro A, Lohmann SM, Evain-Brion D, Tasken K. Mitosis-specific phosphorylation and subcellular redistribution of the RIIalpha regulatory subunit of cAMP-dependent protein kinase. J Biol Chem 1998;273:34594–34602.
21. Gangal M, Li F, Jones JM, Deich J, Lovett K, Taylor SS, Johnson DA. Consequences of cAMP and catalytic subunit binding on the flexibility of the A-kinase regulatory subunit. Biochemistry 2000; 39:15626–15632.
22. Diller TC, Xuong N-h, Taylor SS. Type IIβ regulatory subunit of cAMP-dependent protein kinase: Purification strategies to optimize crystallization. Protein Expr Purif 2000;20:357–364.
23. Builder SE, Beavo JA, Krebs EG. Stoichiometry of cAMP and 1,N6-etheno-cAMP binding to protein kinase. J Biol Chem 1980; 225:2350–2354.
24. Lakowicz JR. Principles of fluorescence spectroscopy. New York: Plenum; 1983. 496 p.
25. Pace CN. Determination and analysis of urea and guanidine hydrochloride denaturation curves. Methods Enzymol 1986;131: 266–280.
26. Chen RF. Fluorescence quantum yields of tryptophan and tyrosine. Anal Lett 1967;1:35–42.
27. Beechem J. A second generation global analysis program for the recovery of complex inhomogeneous fluorescence decay kinetics. Chem Phys Lipids 1989;50:237–251.
28. Chen Y, Liu B, Yu HT, Barkley, MD. The peptide bond quenches indole fluorescence. J Am Chem Soc 1996;118:9271–9278.
29. Chen RF, Knutson JR, Ziffer H, Porter D. Fluorescence of tryptophan dipeptides: correlations with the rotamer model. Biochemistry 1991;30:5184–5195.
30. Carrasco B, de la Torre, JG. Improved hydrodynamic interaction in macromolecular bead models. J Chem Phys 1999;111:4817–4826.
31. Zhao J, Hoye E, Boylan S, Walsh DA, Trewhella J. Quaternary structures of a catalytic subunit-regulatory subunit dimeric complex and the holoenzyme of the cAMP-dependent protein kinase by neutron contrast variation. J Biol Chem 1998;273:30448–30459.
32. Shen X, Knutson JR. Subpicosecond fluorescence spectra of tryptophan in water. J Phys Chem B 2001;105:6260–6265.
33. Eftink MR. The use of fluorescence methods to monitor unfolding transitions in proteins. Biophys J 1994;66:482–501.
34. Leon DA, Canaves JM, Taylor SS. Probing the multidomain structure of the type I regulatory subunit of cAMP-dependent protein kinase using mutational analysis: Role and environment of endogenous tryptophans. Biochemistry 2000;39:5662–5671.
35. LaPorte DC, Builder SE, Storm DR. Spectroscopic studies of the

cAMP binding sites of the regulatory subunits of type I and II protein kinase. J Biol Chem 1980;255:2343–2349.
36. Potter RL, Taylor SS. Relationships between structural domains and function in the regulatory subunit of cAMP-dependent protein kinases I and II from porcine skeletal muscle. J Biol Chem 1979;254:2413–2418.
37. Potter RL, Taylor SS. Correlation of the cAMP binding domain with a site of autophosphorylation on the regulatory subunit of cAMP-dependent protein kinase II from porcine skeletal muscle. J Biol Chem 1979;254:9000–9005.
38. Dell'Acqua ML, Scott, JD. Protein kinase A anchoring. J Biol Chem 1997;272:12881–12884.
39. Herberg FW, Zimmermann B, McGlone M, Taylor SS. Importance of the A-helix of the catalytic subunit of cAMP-dependent protein kinase for stability and for orienting subdomains at the cleft interface. Prot Sci 1997;6:569–579.
40. Gangal M, Clifford T, Deich J, Cheng X, Taylor SS, Johnson DA. Mobilization of the A-kinase N-myristate through an isoform-specific intermolecular switch. Proc Natl Acad Sci USA 1999;96: 12394–12399.
41. Cheng X, Phelps C, Taylor SS. Differential binding of cAMP-dependent protein kinase regulatory subunit isoforms Ialpha and IIbeta to the catalytic subunit. J Biol Chem 2001;276:4102–4108.